

A 2- μm BiCMOS Rectifier-Free AC–DC Piezoelectric Energy Harvester-Charger IC

Dongwon Kwon, *Student Member, IEEE*, and Gabriel A. Rincón-Mora, *Senior Member, IEEE*

Abstract—A fundamental problem that miniaturized systems, such as biomedical implants, face is limited space for storing energy, which translates to short operational life. Harvesting energy from the surrounding environment, which is virtually a boundless source at these scales, can overcome this restriction, if losses in the system are sufficiently low. To that end, the 2- μm bi-complementary metal–oxide semiconductor switched-inductor piezoelectric harvester prototype evaluated and presented in this paper eliminates the restrictions associated with a rectifier to produce and channel 30 μW from a periodic 72- μW piezoelectric source into a battery directly. In doing so, the circuit also increases the system’s electrical damping force to draw more power and energy from the transducer, effectively increasing its mechanical-electrical efficiency by up to 78%. The system also harnesses up to 659 nJ from nonperiodic mechanical vibrations, which are more prevalent in the environment, with $6.1 \pm 1.5\%$ to $8.8 \pm 6.9\%$ of end-to-end mechanical-electrical efficiency.

Index Terms—Battery charger, biomedical implant, body-sensor network, energy harvesting, harvester, piezoelectric, rectifier free, switched-inductor converter, vibration, wireless microsensor.

I. PIEZOELECTRIC ENERGY HARVESTERS

MINATURIZED mobile-electronic systems, such as biomedical drug-delivery implants [1], acceleration- and pressure-monitoring sensors [2], [3], and microsensor nodes in body-sensor networks [4], [5], have so little space for energy storage that they suffer from short operational lives. Unfortunately, replacing easily exhaustible onboard batteries is prohibitive because the systems often conduct *in situ* measurements in unreachable places, such as in the human body, and operate in concert with numerous other devices [5], where the personnel, risks, and logistical costs of maintaining all batteries charged are unacceptably high. Harvesting energy, however, from light [6]; heat [7], [8]; radiation [9]; and motion [10]–[12] is an attractive, though not easy alternative for replenishing small batteries and capacitors.

Although the application ultimately determines what energy source suits best, harvesting kinetic energy is promising because motion and vibrations are abundant (in the ankle, for example) and produce moderate power levels. For context, solar light generates more power, but only when exposed directly to the sun, and power densities derived from indoor lighting, thermal gradients, and radio-frequency (RF) waves fall well below their

Manuscript received June 11, 2010; accepted August 24, 2010. Date of publication October 28, 2010; date of current version November 24, 2010. This work was supported by Linear Technology Corporation. This paper was recommended by Associate Editor A. Hamoui.

The authors are with the School of Electrical and Computer Engineering, Georgia Tech Analog, Power, and Energy IC Research Lab, Georgia Institute of Technology, Atlanta, GA 30332 USA (e-mail: dkwon3@gatech.edu; Rincon-Mora@gatech.edu).

Color versions of one or more of the figures in this paper are available online at <http://ieeexplore.ieee.org>.

Digital Object Identifier 10.1109/TBCAS.2010.2077288

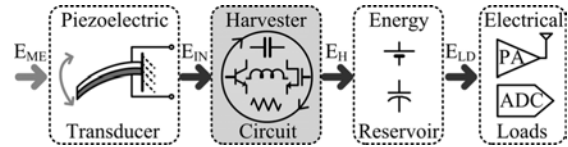


Fig. 1. Harvesting mechanical energy from piezoelectric transducers.

kinetic counterparts [11], [12], although not all motion-based transducers perform equally well. Piezoelectric devices, in fact, when constrained to small platforms, generate more power than variable (electrostatic) capacitors and moving (electromagnetic) coils [11]–[13].

When considering a piezoelectric source, as shown in Fig. 1, the internal charge configuration of the material changes (very similar to an ac current source) to generate an alternating voltage across the equivalent capacitance that its opposing surfaces present [13]. The harvester circuit must therefore extract energy from the changing voltages of the piezoelectric capacitor and deposit charge into an energy-storage device. Since harvested power is low and uncorrelated to the load, a small battery or capacitor serves as the reservoir from which electrical functions in the system draw power on demand.

Conventional approaches first rectify the incoming ac voltage with a diode bridge. References [14] and [15] reduce the voltage (and, therefore, power losses) across the pn-junction diodes by using metal–oxide semiconductor (MOS) switches and drive them with a comparator that senses and ensures only small positive terminal voltages, allowing the switches to close. Unfortunately, input voltages must nonetheless exceed their rectified outputs for the MOS switches to conduct, which means rectifiers inevitably place a threshold limit on the mechanical input. In other words, rectified harvesters only harvest energy above a minimum input level, so they cannot extract all of the energy the piezoelectric material offers. Although [16]–[20] extract more energy from the environment by boosting the transducer’s electrical damping force with higher (LC-induced) piezoelectric voltages, the subsequent rectifier still suffers from a threshold minimum below which the harvester cannot harness energy. Furthermore, drawing maximum power requires an optimal rectified output voltage, so [21], [22], at the cost of power, employs a correcting feedback loop that senses the harvester’s output current to set the optimal rectified level.

A minimum threshold imposed by rectifiers is ultimately a significant fundamental limit under microscale dimensions because: 1) miniaturized piezoelectric transducers, by default, generate low voltages [23]–[26] and 2) weak vibrations, which also produce low power, are prevalent in the environment. The underlying aim of the proposed harvester is to eliminate the rectifier and its resulting low-voltage limitation. Another important advantage of the circuit is that it augments, similar to [16]–[20] but without a rectifier, the electrical damping

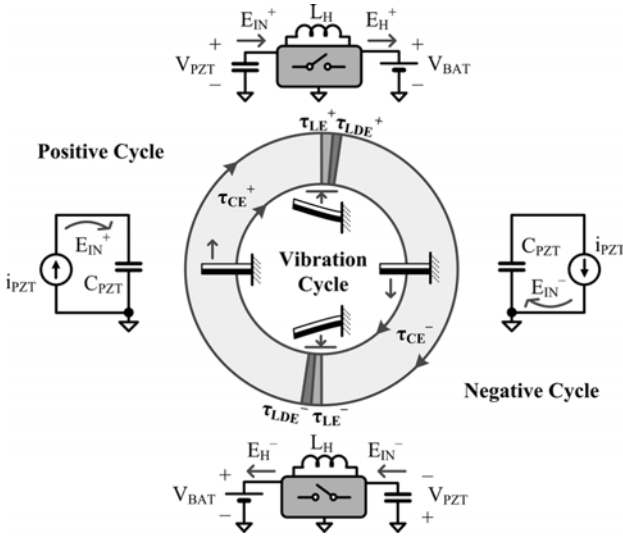


Fig. 2. Full-cycle operation of the proposed piezoelectric harvester.

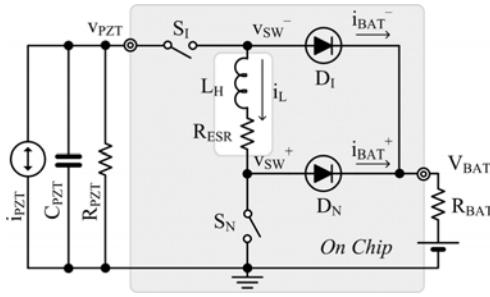


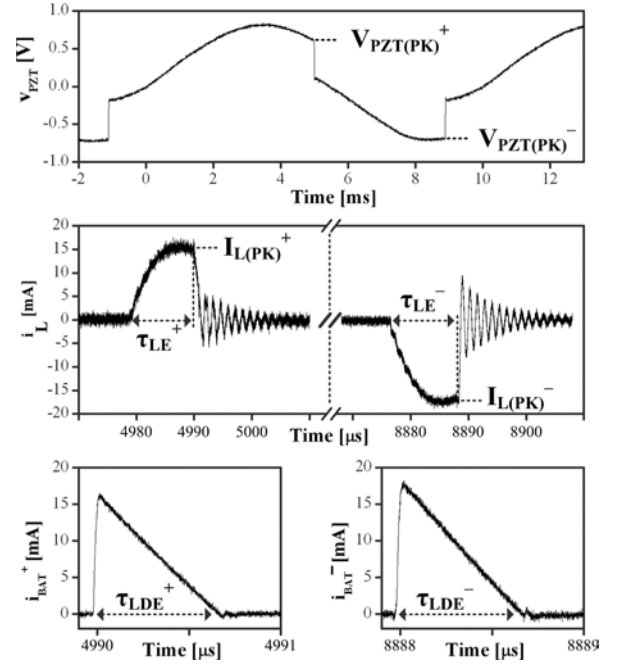
Fig. 3. Simplified schematic of the switched-inductor power stage.

force that it presents to the transducer to induce the system to draw more energy from the environment, effectively increasing the mechanical-electrical (and end-to-end) efficiency of the transducer (and system). To that end, while [27] presented the simulation results of the proposed power stage and [28] briefly reported partial experimental performance from the prototyped power stage and its control circuit, Section II of this paper details how the prototype system operates across a cycle and how it induces the transducer to harness more energy from the environment. Section III then describes in depth the integrated-circuit (IC) implementation and Sections IV and V illustrate the charging and efficiency performance of the prototype with periodic and nonperiodic mechanical inputs (i.e., vibrations), drawing relevant conclusions in Section VI.

II. PROPOSED HARVESTER-CHARGER SYSTEM

A. Energy Flow

Fig. 2 graphically illustrates how the proposed harvester operates and transfers energy across a vibration cycle. When vibrations move the piezoelectric cantilever in the positive cycle, for example, the system waits until the voltage across piezoelectric capacitance C_{PZT} peaks, which occurs when the transducer's cantilever reaches its maximum displacement. At this point, the system energizes the harvesting inductor L_H from C_{PZT} in energizing time τ_{LE}^+ and then de-energizes L_H into the battery in de-energizing time τ_{LDE}^+ . Transferring energy this


 Fig. 4. Experimental time-domain waveforms of the piezoelectric voltage v_{PZT} , inductor current i_L , and the de-energizing (battery) currents i_{BAT}^+ and i_{BAT}^- .

way only requires a few microseconds, which represents a negligible fraction of the millisecond vibration period, so the position of the transducer is, for all practical purposes, static during the transfer. Similarly, after depositing positive-cycle charge into the battery, the system waits until the piezoelectric device charges C_{PZT} in the negative direction to its negative peak. The switched-inductor circuit then quickly energizes and de-energizes L_H in τ_{LE}^- and τ_{LDE}^- from C_{PZT} to the battery. This negative-cycle transfer concludes the cycle, and the sequence repeats as long as vibrations persist.

C_{PZT} stores the energy that the piezoelectric material produces each half cycle (E_{IN}^+) and the switched-inductor converter extracts E_{IN}^+ from C_{PZT} to reset C_{PZT} 's voltage v_{PZT} to 0 V. Assuming piezoelectric current i_{PZT} is sinusoidal at $I_{PZT} \sin(\omega_{VIB}t)$, v_{PZT} during the positive-cycle time, τ_{CE}^+ is

$$\begin{aligned} v_{PZT}(t) &= \frac{1}{C_{PZT}} \int_0^t i_{PZT}(\tau) d\tau \\ &= \left(\frac{I_{PZT}}{\omega_{VIB} C_{PZT}} \right) [1 - \cos(\omega_{VIB}t)]. \end{aligned} \quad (1)$$

Therefore, after τ_{CE}^+ , C_{PZT} accumulates

$$E_{IN}^+ \approx \int_0^{\tau_{CE}^+ \approx T/2} i_{PZT}(t) v_{PZT}(t) dt = \frac{2I_{PZT}^2}{\omega_{VIB}^2 C_{PZT}}. \quad (2)$$

Since the negative cycle generates an equivalent amount (i.e., $E_{IN}^+ \approx E_{IN}^-$), the system harnesses $4I_{PZT}^2/\omega_{VIB}^2 C_{PZT}$ from each vibration period, which is four times ($4 \times$) more energy than the ideal diode-rectified case can possibly induce [21].

B. Time-Domain Operation

In the positive cycle, with switch S_1 open, the switched-inductor power stage in Fig. 3 waits for i_{PZT} to charge C_{PZT} to

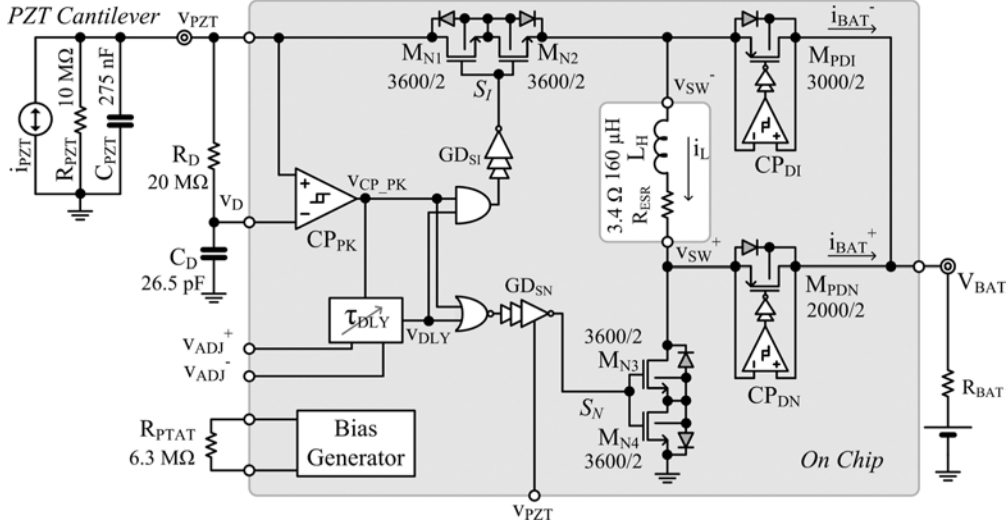


Fig. 5. Prototyped piezoelectric energy harvester IC (in gray) and system (transistor dimensions are in micrometers).

peak positive voltage $V_{PZT(PK)}^+$, as the experimental waveforms of Fig. 4 illustrate. $V_{PZT(PK)}^+$ is not the actual peak because the implemented circuit includes delay and offset, the causes and implications of which subsequent subsections will address. The controller then closes S_I and S_N to energize L_H from C_{PZT} for energizing time τ_{LE}^+ , allowing L_H 's current i_L to reach positive peak current $i_{L(PK)}^+$. Since a capacitor fully discharges into an inductor in a quarter of its LC resonance period, the system sets τ_{LE}^+ to one-fourth of $2\pi\sqrt{(L_H C_{PZT})}$. After τ_{LE}^+ , S_N opens and i_L charges the parasitic capacitance at v_{SW}^+ until the noninverting diode D_N forward biases and steers i_L 's de-energizing (battery) current i_{BAT}^+ into the battery. Once D_N completely drains L_H , after de-energizing time τ_{LDE}^+ , D_N opens automatically (i.e., asynchronously).

The negative cycle operates similarly, except the power stage inverts its functionality to realize an inverting buck-boost translation. As such, the system waits for i_{PZT} to charge C_{PZT} in the negative direction until v_{PZT} reaches negative peak voltage $V_{PZT(PK)}^-$. (Similar to before, $V_{PZT(PK)}^-$ is not accurate because of nonidealities in the circuit.) S_I and S_N then discharge C_{PZT} into L_H for one-fourth of L_H - C_{PZT} 's resonance period, after which point S_I opens and i_L charges v_{SW}^- 's parasitic capacitance until inverting diode D_I forward biases and conducts i_L 's de-energizing (battery) current i_{BAT}^- into the battery.

Unlike rectifier-based harvesters, the proposed switched-inductor circuit can de-energize (and, therefore, harness) all piezoelectric energy in C_{PZT} , which is to say the circuit does not suffer from a minimum input threshold. What is more, L_H automatically raises v_{SW}^+ and v_{SW}^- to whatever voltage the battery demands, which means the circuit does not require the additional dc-dc converter stage that [20]–[22] uses to drive charge into the battery. Unlike the converters in [21] and [22], which include a lossy feedback loop to adjust the rectifier output voltage to draw the maximum power from C_{PZT} , the proposed harvester can derive four times ($4\times$) more energy than rectified harvesters without a correcting loop.

III. IC DESIGN

The prototyped harvester shown in Fig. 5 integrates the switches, controller, and bias generator into a single 2- μm

BiCMOS IC. Bias resistor R_{PTAT} and delay filter elements R_D and C_D are off-chip for testing flexibility. For the same reasons, external voltages v_{ADJ}^+ and v_{ADJ}^- adjust energizing times τ_{LE}^+ and τ_{LE}^- externally. The piezoelectric cantilever, the battery, and L_H are also off-chip.

A. Switches and Gate Drivers

A series combination of two NMOS transistors in an isolated p-well implements S_I and S_N in Fig. 5. The purpose of the back-to-back body diodes is to block the undesired diode current that would otherwise result through the body diode of a single transistor when v_{PZT} swings below ground (in the negative cycle) or above battery voltage V_{BAT} (in the positive cycle). Note that the series combination of two switches increases channel resistance and gate capacitance, which raise conduction and switching losses, respectively, but not to the extent body-diode conduction would dissipate power.

Allowing v_{PZT} to swing below ground demands that S_N 's gate driver GD_{SN} output a negative voltage. The reason for this is that while S_N is open during the negative cycle, when v_{PZT} falls below ground, S_I remains closed and, as a result, switch-node voltages v_{SW}^+ and v_{SW}^- follow v_{PZT} below ground. During this time, driving S_N 's gate to zero would not disengage S_N . To avoid this problem, GD_{SN} 's last inverter stage connects to v_{PZT} instead of ground, as Fig. 6(a) shows. Accordingly, as the simulation results of Fig. 6(b) illustrate, GD_{SN} 's output v_{GDSN_OUT} follows v_{PZT} during the negative cycle and nears V_{BAT} otherwise. Since S_N 's gate capacitance is orders of magnitude below C_{PZT} 's, GD_{SN} hardly drains C_{PZT} , that is, it has a negligible impact on v_{PZT} . However, when the system raises v_{GDSN_OUT} to V_{BAT} (to close S_N and energize L_H), inverter M_{PGD3} - M_{NGD3} conducts considerable shoot-through current (for about 50 ns) because M_{NGD3} 's source voltage v_{PZT} rises more slowly (in τ_{LE}^-) than M_{NGD3} 's gate voltage drop to zero (in a few nanoseconds). To minimize this loss, M_{NGD3} 's width-length aspect ratio W/L is relatively low to increase resistance, yet high enough to open S_N in time to drain L_H into the battery (with i_{BAT}^+).

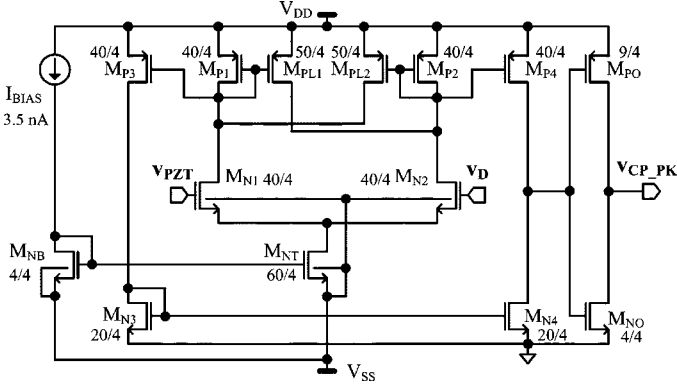


Fig. 8. Peak-detecting comparator CP_{PK} (dimensions are in micrometers and body terminals connect to their respective supplies, unless otherwise specified).

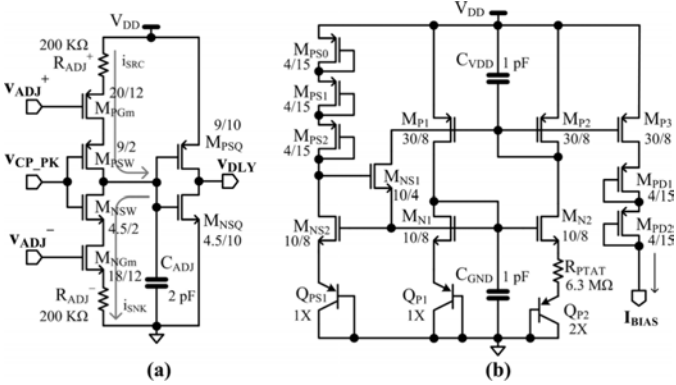


Fig. 9. (a) Adjustable delay τ_{DLY} and (b) PTAT current-generator circuits (dimensions are in micrometers) and body terminals connect to their respective supplies, unless otherwise specified).

the ensuing inverter in $1/2\pi\sqrt{(L_H C_{PZT})}$. Since tolerance in R_{ADJ} and C_{ADJ} offset this time, and other parasitic effects similarly shift how long C_{PZT} should discharge into L_H , v_{ADJ}^+ and v_{ADJ}^- are adjustable (and off-chip for testing flexibility). Notice that M_{NSQ} and M_{PSQ} dissipate shoot-through power because C_{ADJ} 's voltage rises and falls at relatively low rates, so to reduce this loss, their channel lengths are relatively long at $10 \mu\text{m}$. In case tuning the effective R-C time constants externally is prohibitive, monitoring L_H 's voltage v_L with a comparator so that it trips when v_L (which is equal to $L_H di_L/dt$) crosses zero (when i_L peaks) can alternately set L_H 's energizing times τ_{LE}^+ and τ_{LE}^- . Note, however, L_H 's equivalent-series resistance (ESR) is parasitic and must therefore remain negligibly low to minimize the timing error and harvesting-performance degradation it produces.

The nanoamp generator shown in Fig. 9(b) biases CP_{PK} . Operationally, one-to-one mirror M_{P2} - M_{P1} and gate-coupled pair M_{N1} - M_{N2} ensure the M_{N1} - M_{N2} 's source voltages are equal. As a result, the area ratio between Q_{P2} and Q_{P1} establishes proportional-to-absolute-temperature (PTAT) diode-voltage difference ΔV_D across R_{PTAT} to set I_{BIAS} to

$$I_{BIAS} = \frac{\Delta V_D}{R_{PTAT}} = \frac{V_t \ln \left(\frac{I_{P1} A_2}{I_{P2} A_1} \right)}{R_{PTAT}} = \frac{V_t \ln 2}{R_{PTAT}} \quad (3)$$

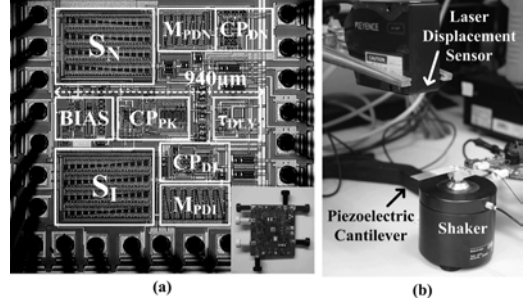


Fig. 10. (a) Die and PCB (inset). (b) Test setup of the prototyped harvester.

which is supply independent. Here, V_t is the thermal voltage and I_{P1} - I_{P2} and A_1 - A_2 are Q_{P1} - Q_{P2} 's currents and areas, respectively. R_{PTAT} 's large off-chip resistance (at $6.3 \text{ M}\Omega$) ensures I_{BIAS} is in the nanoamp range. Note I_{BIAS} is only PTAT if R_{PTAT} has a low-temperature coefficient, which is not a requirement for this circuit. Without startup transistor M_{NS1} , the circuit is stable at either the previously defined I_{BIAS} or zero, when M_{P1} - M_{P2} is off and Q_{P1} - Q_{P2} 's voltages are zero. M_{NS1} forces the circuit into its on state because M_{NS1} 's gate-source voltage would otherwise be high enough (as defined by M_{PS0} , M_{PS1} , M_{PS2} , M_{NS2} , and Q_{PS1}) to steer current from M_{P1} into M_{N1} . Incidentally, diode-connected PMOS transistors M_{PD1} and M_{PD2} level-shift CP_{PK} 's current-bias terminal voltage (across M_{NB} in Fig. 8) to decrease channel-length modulation errors in M_{P3} .

IV. CHARGING AND EFFICIENCY PERFORMANCE

Fig. 10(a) illustrates the fabricated $940 \times 960\text{-}\mu\text{m}^2$ $2\text{-}\mu\text{m}$ BiCMOS integrated circuit (IC) and its corresponding printed-circuit-board (PCB) prototype. The measured inductance and ESR of the $4.4 \times 4.4 \times 1.4\text{-mm}^3$ Coilcraft LPS4414 inductor were $160 \mu\text{H}$ and 3.4Ω . The Brüel & Kjær's Mini-Shaker 4810 shown in Fig. 10(b) generated the 100-Hz periodic vibrations used to stimulate the $44 \times 13 \times 0.4\text{-mm}^3$ piezoelectric cantilever at its resonant frequency. A laser-displacement sensor measured the vertical position of the cantilever to study the relationship between mechanical and electrical parameters. The amplitude of the transducer's open-circuit voltage $\Delta v_{PZT(\text{UNLOADED})}$ and the cantilever's acceleration rate rises almost linearly with shaker-vibration strength. For example, $\Delta v_{PZT(\text{UNLOADED})}$ is 0.35, 0.5, 0.7, and 0.9 V when the acceleration at the base of the cantilever is 0.048, 0.069, 0.094, and 0.120 m/s^2 and at the tip of the cantilever, it is 3.05, 4.49, 6.44, and 8.34 m/s^2 , respectively.

A. Charging Performance

The prototype successfully charged 160-nF SMD ceramic and $23\text{-}\mu\text{F}$ electrolytic capacitors from inputs with $\Delta v_{PZT(\text{UNLOADED})}$'s of 0.35, 0.5, 0.7, and 0.9 V at successively increasing rates, as Fig. 11 shows. The capacitor voltages rise in staircase fashion because the circuit deposits a small, but fixed amount of energy (from C_{PZT}) every half cycle, much like a (trickle) pulse charger [32]–[34]. As expected, the resulting step size is smaller for $23 \mu\text{F}$ and increases with larger

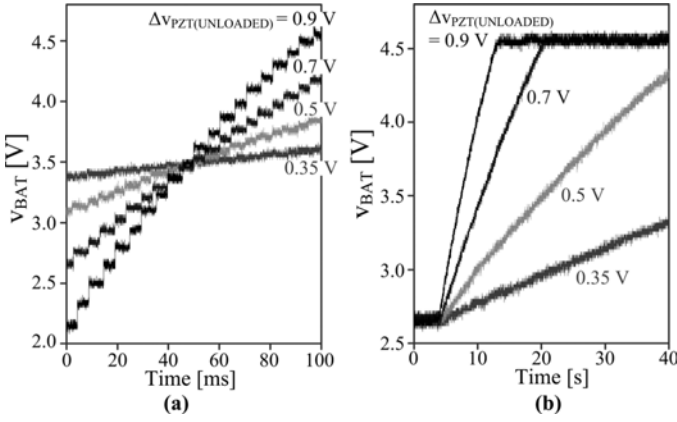


Fig. 11. Experimental time-domain charging profiles for (a) 160-nF SMD ceramic and (b) 23- μF electrolytic capacitors.

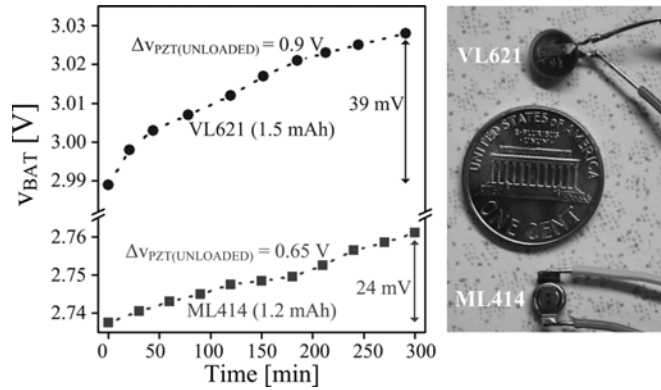


Fig. 12. Experimental time-domain charging profiles for Li-Ion batteries ML414 and VL621.

$\Delta V_{\text{PZT(UNLOADED)}}$'s because stronger mechanical vibrations deposit more energy into C_{PZT} .

Energy per cycle (i.e., step size) is low (and charge time relatively long) because miniaturized harvesters produce little power. As a result, the 1.2- and 1.5-mAh lithium-ion (Li-Ion) batteries in Fig. 12 (i.e., ML414 and VL621) charged from 0.65- and 0.9-V $\Delta V_{\text{PZT(UNLOADED)}}$'s raise their corresponding voltages by 24 and 39 mV in 300 min. For these capacitor and battery-charging experiments, an external low-leakage operational amplifier in the unity-gain configuration monitored V_{BAT} and a low-leakage off-chip diode connected to an external 4-V supply clamped V_{BAT} within the targeted range.

B. Conversion Efficiency

After discounting losses, the system harnesses up to 30 μW (P_{H} in Fig. 13) from 72 μW of transducer-generated power ($P_{\text{IN(LOADED)}}$). Without the harvester (i.e., unloaded) and under equal mechanical stimulation, the energy per cycle in C_{PZT} (i.e., $C_{\text{PZT}}\Delta V_{\text{PZT(UNLOADED)}}^2 f_{\text{VIB}}$) can generate less power ($P_{\text{IN(UNLOADED)}}$) than when loaded (e.g., 40 versus 72 μW). This is the result, as expected, because extracting all C_{PZT} 's positive- and negative-cycle energy resets (i.e., conditions) v_{PZT} to zero, further increasing the transducer's electrical damping force and thereby inducing it to derive more energy from the environment. Note that $P_{\text{IN(UNLOADED)}}$ also represents the maximum input power a rectifier-based

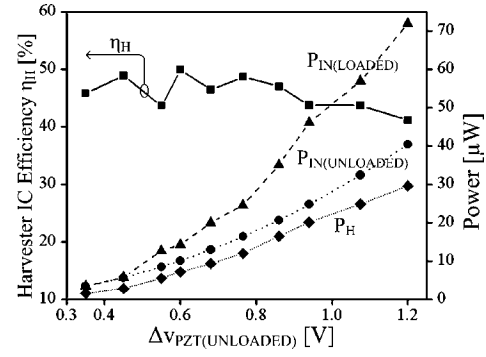


Fig. 13. Measured conversion efficiency η_{H} , input and output power $P_{\text{IN(LOADED)}}$, and P_{H} , and unloaded input power $P_{\text{IN(UNLOADED)}}$ across mechanical vibration strength (i.e., across C_{PZT} 's $\Delta V_{\text{PZT(UNLOADED)}}$) at 100 Hz.

circuit can produce because a rectifier draws charge from C_{PZT} without conditioning its voltage. In other words, the best possible (and ideal) rectifier-based system would draw roughly 56% of what the proposed harvester can (e.g., 40 of 72 μW).

Although increasing the transducer's output power by up to 78% or $1.78\times$ (when $\Delta V_{\text{PZT(UNLOADED)}}$ is 1.2 V) by loading it with the prototyped harvester corroborates theory, (2) predicts a $4\times$ (i.e., 400%) improvement. One reason for this discrepancy is C_{PK} 's 36-mV input-referred offset causes the system to discharge C_{PZT} past v_{PZT} 's peak, as already mentioned and shown in Fig. 4, after C_{PZT} loses some energy to vibrations. What is more, since the offset voltage does not scale with the input, the fraction of energy lost to vibrations is larger for smaller inputs, so loaded-to-unloaded input-power ratio $P_{\text{IN(LOADED)}/P_{\text{IN(UNLOADED)}}$ decreases from 1.78 rapidly (i.e., nonlinearly) with respect to $\Delta V_{\text{PZT(UNLOADED)}}$. Parasitic resistances in switches S_{N} and S_{I} and across L_{H} (in Figs. 3 and 5) also reduce the transducer's output power because, instead of fully draining C_{PZT} into L_{H} by lowering v_{PZT} to zero, the converter pulls v_{PZT} to the voltage drop across S_{N} , L_{H} , and S_{I} 's combined series resistance $R_{\text{SN}} + R_{\text{ESR}} + R_{\text{SI}}$. This nonzero voltage not only represents remnant energy that the system does not harvest but also lowers the peak amplitude (i.e., electrical damping force) of the ensuing half cycle.

Ultimately, the harvesting conversion efficiency of the system with respect to $P_{\text{IN(LOADED)}}$ (η_{H} in Fig. 13) across vibration strength falls between 40% and 50%. The system loses conduction energy E_{C} to the switches' finite resistances and L_{H} 's ESR when i_{L} flows through L_{H} during L_{H} 's positive- and negative-cycle energizing and de-energizing times τ_{LE}^+ , τ_{LDE}^+ , τ_{LE}^- , and τ_{LDE}^- . However, as Fig. 4 shows, L_{H} de-energizes in considerably less time than it energizes (i.e., τ_{LE}^+ and τ_{LE}^- are considerably longer than τ_{LDE}^+ and τ_{LDE}^-) so E_{C} mostly consists of energizing losses

$$E_{\text{C}} \approx E_{\text{C(LE)}} \approx \left[\left(\frac{I_{\text{L(PK)}}^+}{\sqrt{3}} \right)^2 + \left(\frac{I_{\text{L(PK)}}^-}{\sqrt{3}} \right)^2 \right] \cdot (R_{\text{SI}} + R_{\text{SN}} + R_{\text{ESR}}) \tau_{\text{LE}} \quad (4)$$

where energizing times τ_{LE}^+ and τ_{LE}^- equal (to τ_{LE}) and $I_{\text{L(PK)}}^+/\sqrt{3}$ and $I_{\text{L(PK)}}^-/\sqrt{3}$ are the rms currents flowing through the resistors across τ_{LE}^+ and τ_{LE}^- , respectively. E_{C} falls with increasing L_{H} values because, even though τ_{LE} increases

with $L_H^{0.5}$ (from $1/2\pi\sqrt{L_H C_{PZT}}$), $(I_{L(PK)}^+)^2$, and $(I_{L(PK)}^-)^2$ decreases with L_H^1 . Wider MOS transistors (i.e., lower R_{SI} and R_{SN}) also decrease E_C , but at the expense of silicon real estate and higher switching gate-drive losses $E_{SW(GD)}$, as the following discussion will elucidate.

The system loses $E_{SW(GD)}$ in inverter drivers when they charge and discharge parasitic gate capacitances in S_I , S_N , and D_N , and D_I 's M_{PDN} and M_{PDI} (from Fig. 5). Since all of the switches in the proposed harvester engage and disengage once per cycle, gate-drive losses amount to

$$E_{SW(GD)} \approx (C_{SI} + C_{DI} + C_{DN}) V_{DD}^2 + C_{SN} (V_{DD} + |V_{PZT(PK)}^-|)^2 \quad (5)$$

where C_{SI} , C_{DI} , C_{DN} , and C_{SN} refer to the parasitic capacitances that S_I , D_I 's M_{PDI} , D_N 's M_{PDN} , and S_N introduce, respectively, which scale with transistor channel widths. Note S_N causes more energy loss than the other switches because its gate swings between V_{DD} and $V_{PZT(PK)}^-$.

The system also loses overlap losses $E_{SW(IV)}$ when MOS drain currents and drain-source voltages shortly overlap every time they transition. In the prototyped system, this overlap occurs when S_N and S_I open because v_{SW}^+ and v_{SW}^- transition with a nonzero i_L

$$E_{SW(IV)} \approx (0.5I_{L(PK)}^+ \tau_{SN_OFF} + 0.5I_{L(PK)}^- \tau_{SI_OFF}) \cdot (V_{BAT} + V_D) \quad (6)$$

where V_D refers to M_{PDN} and M_{PDI} 's body-diode voltage. Here, because i_L is triangular and τ_{SN_OFF} and τ_{SI_OFF} are S_N and S_I 's corresponding off times, $0.5I_{L(PK)}^+ \tau_{SN_OFF}$ and $0.5I_{L(PK)}^- \tau_{SI_OFF}$ represent S_N and S_I 's total conducted charge during transitions.

The peak-detector comparator CP_{PK} , the nanoamp-bias generator, adjustable delay block τ_{ADJ} , the logic gates, and D_N and D_I 's comparators CP_{DN} and CP_{DI} in Fig. 5 also dissipate quiescent energy (E_Q). The losses in CP_{PK} and the bias circuit, however, dominate E_Q because they operate through the entire vibration cycle, whereas the other circuits only engage for a substantially smaller fraction. Overall, although higher input power increases $|V_{PZT(PK)}^-|$, $I_{L(PK)}^+$, and $I_{L(PK)}^-$, and their associated switching losses $E_{SW(GD)}$ and $E_{SW(IV)}$, conduction losses E_C scale more rapidly with power (i.e., proportional to $(I_{L(PK)}^+)^2$ and $(I_{L(PK)}^-)^2$) so E_C ultimately dominates and limits η_H when mechanical vibrations are strong. Conversely, when vibrations are weak, E_Q can dominate because E_C , $E_{SW(GD)}$, and $E_{SW(IV)}$ scale with power. Similarly, E_Q can also dominate when the frequency of the input vibration is low because, since the harvester synchronizes itself to a lower vibration period, E_C , $E_{SW(GD)}$, and $E_{SW(IV)}$ decrease accordingly. A fundamental challenge here is that E_Q remains constant so η_H degrades with decreasing strength and vibrations.

The increase in η_H with decreasing vibration strength (i.e., $\Delta V_{PZT(UNLOADED)}$'s) across the upper half of the tested range (in Fig. 13) indicates conduction losses E_C dominate because E_C scales more rapidly with strength than output power P_H does. Through the lower range, η_H is for the most part even, which implies that switching losses $E_{SW(GD)}$ and $E_{SW(IV)}$ overwhelm other losses in that region because linear reductions in $E_{SW(GD)}$ and $E_{SW(IV)}$ offset (and balance) linear drops in

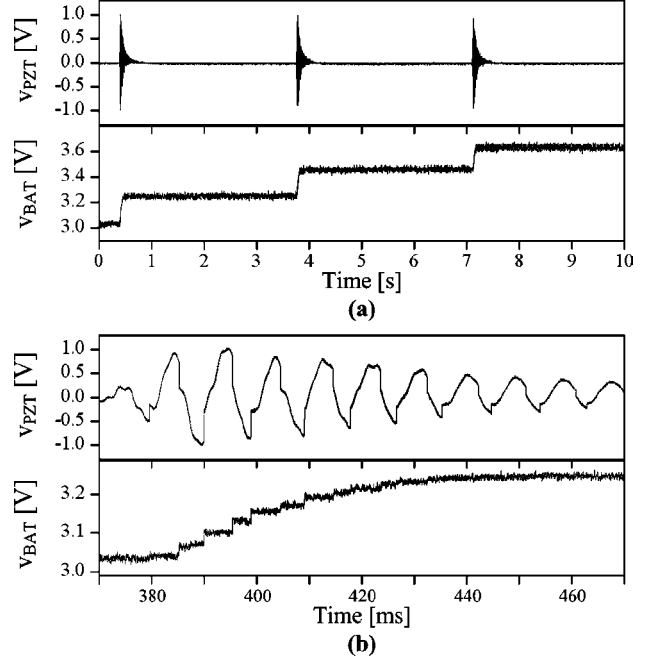


Fig. 14. (a) Second and (b) millisecond (magnified) responses to the impact of a baseball bouncing off a table.

P_H . Since η_H does not fall noticeably with decreasing mechanical strength, quiescent losses E_Q do not appear to dominate. Given all of this, increasing η_H in the upper range is possible by increasing S_I and S_N 's channel widths (i.e., decreasing their corresponding resistances) because E_C would decline more than $E_{SW(GD)}$ would increase.

V. PERFORMANCE UNDER PRACTICAL OPERATING CONDITIONS

Vibrations in practical operating environments occur, for the most part, at relatively low frequencies, between maybe 1 Hz for a person walking to 167 Hz for an engine cycling at 10 000 revolutions per minute. What is more, the rate is often inconsistent and maybe even nonrecurring, as in the case of human motion, wind-propelled movements, and vibrations generated from impact [35]. What all of this means is matching the narrowband of a transducer to vibrations, which is the recipe for high conversion efficiency, is often impractical and unrealistic.

Since the prototyped harvester automatically detects when to draw energy from C_{PZT} , the proposed system is capable of harnessing energy from nonperiodic stimuli. When dropping a 145-g official major-league baseball from 40 cm above the experimental setup table in Fig. 10(b), for example, the impact of the ball bouncing once off the table induces the piezoelectric cantilever to vibrate and produce the pulse train in Fig. 14(a)–(b). In this case, the prototyped system charged 500 nF (from 3.04 V) from a single bounce for three separate trials by roughly 200 mV.

Each drop produces the decaying vibrations. Fig. 14(b) illustrates where the system harvests energy by quickly draining C_{PZT} into L_H and then L_H into the 500-nF capacitor each time v_{PZT} peaks. As v_{PZT} 's peaks (and mechanical strength) decrease, however, the peak-detector comparator CP_{PK} 's offset has a larger impact on how much input power $P_{IN(LOADED)}$ the system harnesses so output power P_H decreases more than basic theory predicts. Under these weak vibrations, in fact, R_D – C_D

and CP_{PK} 's delays increase CP_{PK} 's offset to degrade performance. In contrast, just as CP_{PK} 's offset *adds* to the effects of CP_{PK} 's delay in the positive half-cycle, the offset *Cancels* delay in the negative half-cycle, as Figs. 4 and 14(b) indicate, which means alternating the polarity of the offset can improve overall performance.

Although the immediate aim of this research is to raise P_H by increasing η_H and $P_{IN(LOADED)}$, the ultimate metric is end-to-end harvesting conversion efficiency η_{TOTAL} , which refers to how much mechanical energy E_{ME} reaches the output as harvested energy E_H . The means of applying a known value for E_{ME} (and approximating η_{TOTAL}) is to tie an object of known mass m_W to the tip of the piezoelectric cantilever with a light string and subsequently cut the link. Since the cantilever's elastic force F_C balances the object's gravitational pull F_G , E_{ME} relates to F_G and the cantilever's tip displacement distance d_C

$$E_{ME} = \frac{K_C d_C^2}{2} = \frac{(K_C d_C) d_C}{2} = \frac{F_C d_C}{2} = \frac{F_G d_C}{2} = \frac{(m_W g) d_C}{2} \quad (7)$$

where K_C and g refer to the spring constant and gravity's acceleration, respectively.

This way, neglecting parasitic weights and assuming the string severs instantaneously, the prototyped harvester charged (experimentally) 500 nF by roughly 400 mV, as Fig. 15 shows, from a 3-g weight. As a result, subtracting the external supply's quiescent energy E_Q (to the chip for CP_{PK} , bias generator, adjustable delay, and logic gates) and gate-driving losses $E_{SW(GD)}$ from the energy deposited in the 500-nF capacitor reduces E_H to

$$E_H = 0.5C_{BAT} (V_{BAT(F)}^2 - V_{BAT(I)}^2) - E_Q - E_{SW(GD)} \quad (8)$$

which ranged between 100 and 660 nJ when stimulated with 1.2 to 10.8 μJ of E_{ME} from 1-, 2-, and 3-g weights to yield $6.1 \pm 1.5\%$ to $8.8 \pm 6.9\%$ of η_{TOTAL} or E_H/E_{ME} . Table I summarizes the statistical results (mean and standard deviation) for each weight across 20 trials. To minimize the mechanical disturbance that cutting the link creates, Table I considers only data whose initial peak voltage (v_{PZT}) was small (e.g., less than 100 mV), such as Fig. 15's v_{PZT} .

η_{TOTAL} incorporates the collective performance of the transducer ($\eta_{PZT(LOADED)}$) and the harvester (η_H), which means $P_{ZT(LOADED)}$ is η_{TOTAL}/η_H or roughly 14%–20% when assuming (from Fig. 13) η_H is 45% on average. Since $\eta_{PZT(LOADED)}$ includes a factor improvement that the harvester induces, the unloaded counterpart ($\eta_{PZT(UNLOADED)}$) is less than 14%–20% by up to $1.78 \times$. Although this simple analysis is by no means accurate or complete, it shows that mechanical losses are significant at around 80%, and conditioning the transducer to increase $P_{IN(LOADED)}$ is as important as reducing the losses across the switched-inductor converter (i.e., increasing η_H).

VI. CONCLUSION

The prototyped 2- μm BiCMOS switched-inductor piezoelectric harvester developed, experimentally evaluated, and presented in this paper generates and steers up to 30 μW from a periodic 72- μW piezoelectric source into a capacitor or battery directly. In doing so, it increases the piezoelectric

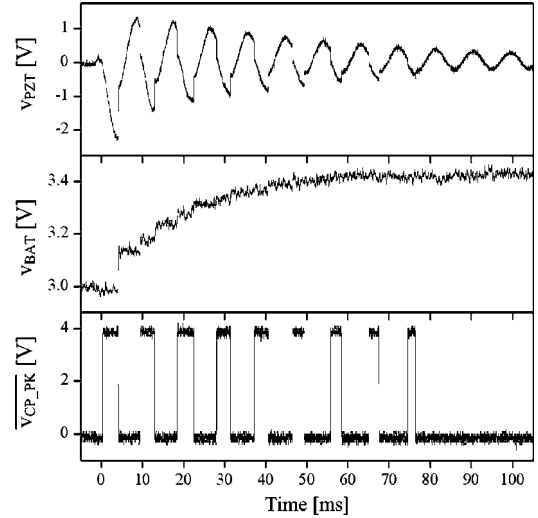


Fig. 15. End-to-end harvesting waveforms for a 3-g weight.

TABLE I
MEASURED MECHANICAL AND NET HARVESTED ENERGY,
AND END-TO-END EFFICIENCIES

| Weight [g] | E_{ME} [nJ] | E_H [nJ] | η_{TOTAL} [%] |
|------------|---------------------|-------------------|--------------------|
| 1 | 1198.0 ± 17.6 | 104.8 ± 82.3 | 8.76 ± 6.89 |
| 2 | 4797.0 ± 123.1 | 402.8 ± 173.3 | 8.39 ± 3.60 |
| 3 | 10792.8 ± 190.3 | 659.1 ± 171.2 | 6.10 ± 1.54 |

cantilever's electrical damping force to raise the transducer's (and, therefore, system's end-to-end) mechanical electrical efficiency by up to 78%. The system also harnesses up to 659 nJ from nonperiodic vibrations with $6.1 \pm 1.5\%$ to $8.8 \pm 6.9\%$ end-to-end mechanical-electrical efficiencies. One key feature of the presented harvester is that it eliminates the need for a rectifier. As a result, the system no longer: 1) places a threshold limit imposed by diodes and/or the output voltage on mechanical vibrations, 2) loses power across an otherwise additional stage (i.e., across a rectifier), and 3) limits how much the circuit dampens the transducer (to produce more power). Conditioning the piezoelectric device to generate more power is an important attribute since it is the relatively simple and low-loss control strategy that the system adopts to energize and de-energize the inductor directly into the energy-storage device. From a practical standpoint, the harvester is also able to harness energy from short, nonperiodic mechanical vibrations, which are more prevalent in real-life applications, such as when someone jumps or suddenly stops, wind gushes, objects crash, and so on.

ACKNOWLEDGMENT

The authors would like to thank Linear Technology Corporation for fabricating the prototyped integrated circuit, and B. Legates and his team for their advice and encouragement.

REFERENCES

- [1] D. A. La Van, T. McGuire, and R. Langer, "Small-scale systems for in vivo drug delivery," *Nature Biotechnol.*, vol. 21, no. 10, pp. 1184–1191, Oct. 2003.

- [2] J. Marek, "MEMS for automotive and consumer electronics," in *Proc. IEEE Int. Solid-State Circuits Conf. Dig. Tech. Papers*, Feb. 2010, vol. 53, pp. 9–17.
- [3] M. Flatscher, M. Dielacher, T. Herndl, T. Lentsch, R. Matischek, J. Prainsack, W. Pribyl, H. Theuss, and W. Weber, "A bulk acoustic wave (BAW) based transceiver for an in-tire-pressure monitoring sensor node," *IEEE J. Solid-State Circuits*, vol. 45, no. 1, pp. 167–177, Jan. 2010.
- [4] J. Yoo, L. Yan, S. Lee, Y. Kim, and H.-J. Yoo, "A 5.2 mW self-configured wearable body sensor network controller and a 12 μ W wirelessly powered sensor for a continuous health monitoring system," *IEEE J. Solid-State Circuits*, vol. 45, no. 1, pp. 178–188, Jan. 2010.
- [5] I. F. Akyildiz, W. Su, Y. Sankarasubramaniam, and E. Cayirci, "Wireless sensor networks: a survey," *Comput. Netw.*, vol. 38, pp. 393–422, 2002.
- [6] N. J. Guilar, T. J. Kleeburg, A. Chen, D. R. Yankelevich, and R. Amirtharajah, "Integrated solar energy harvesting and storage," *IEEE Trans. Very Large Scale Integr. Syst.*, vol. 17, no. 5, pp. 627–637, May 2009.
- [7] H. Lhermet, C. Condemine, M. Plissonnier, R. Salot, P. Audebert, and M. Rosset, "Efficient power management circuit: from thermal energy harvesting to above-IC microbattery energy storage," *IEEE J. Solid-State Circuits*, vol. 43, no. 1, pp. 246–255, Jan. 2008.
- [8] E. J. Carlson, K. Strunz, and B. P. Otis, "A 20 mV input boost converter with efficient digital control for thermoelectric energy harvesting," *IEEE J. Solid-State Circuits*, vol. 45, no. 4, pp. 741–750, Apr. 2010.
- [9] T. Le, K. Mayaram, and T. Fiez, "Efficient far-field radio frequency energy harvesting for passively powered sensor networks," *IEEE J. Solid-State Circuits*, vol. 43, no. 5, pp. 1287–1302, May 2008.
- [10] J. A. Paradiso and T. Starner, "Energy scavenging for mobile and wireless electronics," *Perv. Comput.*, vol. 4, pp. 18–27, 2005.
- [11] P. D. Mitcheson, E. M. Yeatman, G. K. Rao, A. S. Holmes, and T. C. Green, "Energy harvesting from human and machine motion for wireless electronic devices," *Proc. IEEE*, vol. 96, no. 9, pp. 1457–1486, Sep. 2008.
- [12] S. Roundy, P. K. Wright, and J. Rabaey, "A study of low level vibrations as a power source for wireless sensor nodes," *Comput. Commun.*, vol. 26, pp. 1131–1144, 2003.
- [13] S. Priya and D. J. Inman, *Energy Harvesting Technologies*. New York: Springer, 2009. T. Le, J. Han, A. von Jouanne, K. Mayaram, and T. S. Fiez, "Piezoelectric micro-power generation interface circuits," *IEEE J. Solid-State Circuits*, vol. 41, no. 6, pp. 1411–1420, Jun. 2006.
- [14] T. T. Le, J. Han, A. von Jouanne, K. Mayaram, and T. S. Fiez, "Piezoelectric micro-power generation interface circuits," *IEEE J. Solid-State Circuits*, vol. 41, no. 6, pp. 1411–1420, Jun. 2006.
- [15] N. J. Guilar, R. Amirtharajah, and P. J. Hurst, "A full-wave rectifier with integrated peak selection for multiple electrode piezoelectric energy harvesters," *IEEE J. Solid-State Circuits*, vol. 44, no. 1, pp. 240–246, Jan. 2009.
- [16] D. Guyomar, A. Badel, E. Lefeuvre, and C. Richard, "Toward energy harvesting using active materials and conversion improvement by nonlinear processing," *IEEE Trans. Ultrason., Ferroelect., Freq. Control*, vol. 52, no. 4, pp. 584–595, Apr. 2005.
- [17] E. Lefeuvre, A. Badel, C. Richard, and D. Guyomar, "Piezoelectric energy harvesting device optimization by synchronous electric charge extraction," *J. Intell. Mater. Syst. Structures*, vol. 16, pp. 865–876, Oct. 2005.
- [18] A. Badel, D. Guyomar, E. Lefeuvre, and C. Richard, "Piezoelectric energy harvesting using a synchronized switch technique," *J. Intell. Mater. Syst. Structures*, vol. 17, pp. 831–839, Aug./Sep. 2006.
- [19] M. Lallart, L. Garbuio, C. Richard, and D. Guyomar, "Low-cost capacitor voltage inverter for outstanding performance in piezoelectric energy harvesting," *IEEE Trans. Ultrason., Ferroelect., Freq. Control*, vol. 57, no. 2, pp. 281–291, Feb. 2010.
- [20] Y. K. Ramadass and A. P. Chandrakasan, "An efficient piezoelectric energy harvesting interface circuit using a bias-flip rectifier and shared inductor," *IEEE J. Solid-State Circuits*, vol. 45, no. 1, pp. 189–204, Jan. 2010.
- [21] G. K. Ottman, H. F. Hofmann, A. C. Bhatt, and G. A. Lesieutre, "Adaptive piezoelectric energy harvesting circuit for wireless remote power supply," *IEEE Trans. Power Electron.*, vol. 17, no. 5, pp. 669–676, Sep. 2002.
- [22] G. K. Ottman, H. F. Hofmann, and G. A. Lesieutre, "Optimized piezoelectric energy harvesting circuit using step-down converter in discontinuous conduction mode," *IEEE Trans. Power Electron.*, vol. 18, no. 2, pp. 696–703, Mar. 2003.
- [23] W. J. Choi, Y. Jeon, J.-H. Jeong, R. Sood, and S. G. Kim, "Energy harvesting MEMS device based on thin film piezoelectric cantilevers," *J. Electroceram.*, vol. 17, pp. 543–548, 2006.
- [24] M. Renaud, K. Karakaya, T. Sterken, P. Fiorini, C. Van Hoof, and R. Puers, "Fabrication, modelling and characterization of MEMS piezoelectric vibration harvesters," *Sens. Actuators, A Phys.*, vol. 145–146, pp. 380–386, Jul./Aug. 2008.
- [25] N. M. White, P. Glynn-Jones, and S. P. Beeby, "A novel thick-film piezoelectric micro-generator," *Smart Mater. Struct.*, vol. 10, pp. 850–852, 2001.
- [26] B.-S. Lee, S.-C. Lin, and W.-J. Wu, "Comparison of the piezoelectric MEMS generators with interdigital electrodes and laminated electrodes," in *Proc. SPIE-Int. Soc. Opt. Eng.*, Mar. 2008, pp. 69331B-1–69331B-8.
- [27] D. Kwon and G. A. Rincón-Mora, "A rectifier-free piezoelectric energy harvester circuit," in *Proc. IEEE Int. Symp. Circuits and Systems*, May 2009, pp. 1085–1088.
- [28] D. Kwon and G. A. Rincón-Mora, "A single-inductor AC-DC piezoelectric energy-harvester/battery-charger IC converting $\pm(0.35$ to 1.2 V) to $(2.7$ to 4.5 V)," in *Proc. IEEE Int. Solid-State Circuits Conf. Dig. Tech. Papers*, Feb. 2010, vol. 53, pp. 494–495.
- [29] T. Y. Man, P. K. T. Mok, and M. J. Chan, "A 0.9-V input discontinuous-conduction-mode boost converter with CMOS-control rectifier," *IEEE J. Solid-State Circuits*, vol. 43, no. 9, pp. 2036–2046, Sep. 2008.
- [30] Y.-H. Lam, W.-H. Ki, and C.-Y. Tsui, "Integrated low-loss CMOS active rectifier for wirelessly powered devices," *IEEE Trans. Circuits Syst. II, Reg. Papers*, vol. 53, no. 12, pp. 1378–1382, Dec. 2006.
- [31] S. Guo and H. Lee, "An efficiency-enhanced CMOS rectifier with unbalanced-biased comparators for transcutaneous-powered high-current implants," *IEEE J. Solid-State Circuits*, vol. 44, no. 6, pp. 1796–1804, Jun. 2009.
- [32] J. Li, E. Murphy, J. Winnick, and P. A. Kohl, "The effects of pulse charging on cycling characteristics of commercial lithium-ion batteries," *J. Power Sources*, vol. 102, pp. 302–309, 2001.
- [33] Z. Jiang and R. A. Dougal, "Synergetic control of power converters for pulse current charging of advanced batteries from a fuel cell power source," *IEEE Trans. Power Electron.*, vol. 19, no. 4, pp. 1140–1150, Jul. 2004.
- [34] L.-R. Chen, "A design of an optimal battery pulse charge system by frequency-varied technique," *IEEE Trans. Ind. Electron.*, vol. 54, no. 1, pp. 398–405, Feb. 2007.
- [35] F. Cottone, H. Vocca, and L. Gammaitoni, "Nonlinear energy harvesting," *Phys. Rev. Lett.*, vol. 102, pp. 080601-1–080601-4, Feb. 2009.



Dongwon Kwon (S'07) received the B.S. degree in electrical engineering from Seoul National University, Seoul, Korea, in 2003 and the M.S.E.E. degree in electrical engineering from Georgia Institute of Technology, Atlanta, in 2008, where he is currently pursuing the Ph.D. degree.

From 2003 to 2006, he was a Research Engineer with Hantel Inc., Kyunggi, Korea, and developed portable MP3 players. His research interests include piezoelectric energy harvesting circuits, switching-mode power integrated circuits (ICs), and

ultra-low-power analog IC design.

Mr. Kwon won 2nd place in the 2009 Science Applications International Corporation-Georgia Tech student paper competition.



Gabriel A. Rincón-Mora (S'91–M'97–SM'01) received the B.S. degree in electrical engineering from Florida International University, and the M.S. and Ph.D. degrees in electrical engineering from the Georgia Institute of Technology, Atlanta.

He was with Texas Instruments from 1994 to 2003 and was appointed Adjunct Professor at the Georgia Institute of Technology, Atlanta, in 1999–2001, and became a Full-Time faculty member at the Georgia Institute of Technology in 2001. His scholarly products include eight books, one book chapter, more than 125 scientific publications, 27 patents, more than 26 commercial chip designs, and more than 55 international speaking engagements. He was elevated to the grade of Fellow by the Institute of Engineering Technology, inducted into

Georgia Tech's Council of Outstanding Young Engineering Alumni, elected IEEE CASS Distinguished Lecturer for '09-'10, and featured on the cover of Hispanic Business magazine as one of "The 100 Most Influential Hispanics." He has been an Associate Editor for IEEE TRANSACTIONS ON CIRCUITS AND SYSTEMS II: EXPRESS BRIEFS since 2008.

Dr. Rincón-Mora has been an Editorial Board Member for JOLPE since 2009, Chairman of Atlanta's IEEE SSCS-CASS Chapter since 2005, Technical Committee Member for IEEE's CASS ASP and PECAS, Steering Committee Member for IEEE's MWSCAS, was General Chair for SRC's Energy and

Power ICs Workshop in 2009, Circuit Design Vice Chair for IEEE's 2008 ICCDCS; Technical Program Chair for IEEE's 2007 MWSCAS-NEWCAS, Technical Program Co-Chair for IEEE's 2006 MWSCAS, and Vice Chairman of Atlanta's SSCS-CASS Chapter in 2004. He has received the National Hispanic in Technology Award, Charles E. Perry Visionary Award, a Commendation Certificate from the Lieutenant Governor of California, IEEE CASS Service Award, and Robins Air Force Base's "Orgullo Hispano" and "Hispanic Heritage" awards.